AGU PUBLICATIONS

Geophysical Research Letters

RESEARCH LETTER
10.1002/2017GL073294

Key Points:
- Anomalous behavior due spin crossover leads to temperature increments in the adiabats of lower mantle aggregates
- Thermoelastic properties along self-consistent adiabats sharpen uncertainties in analyses of lower mantle composition
- Neglecting the effect of spin crossover would lead to erroneous interpretations of the lower mantle composition and temperature profile

Supporting Information:
- Supporting Information S1

Correspondence to:
R. M. Wentzcovitch,
rmw2150@columbia.edu

Citation:
Valencia-Cardona, J. J., G. Shukla, Z. Wu, C. Houser, D. A. Yuen, and R. M. Wentzcovitch (2017), Influence of the iron spin crossover in ferropericlase on the lower mantle geotherm, *Geophys. Res. Lett.*, *44*, 4863–4871, doi:10.1002/2017GL073294.

Received 6 MAR 2017
Accepted 1 MAY 2017
Accepted article online 5 MAY 2017
Published online 31 MAY 2017

Influence of the iron spin crossover in ferropericlase on the lower mantle geotherm

Juan J. Valencia-Cardona[1], Gaurav Shukla[2], Zhongqing Wu[3], Christine Houser[4], David A. Yuen[1,5], and Renata M. Wentzcovitch[6,7]

[1]Scientific Computing Program, University of Minnesota, Twin Cities, Minneapolis, Minnesota, USA, [2]Department of Chemical Engineering and Materials Science, University of Minnesota, Twin Cities, Minneapolis, Minnesota, USA, [3]School of Earth and Space Sciences, University of Science and Technology of China, Hefei, China, [4]Earth-Life Science Institute, Tokyo Institute of Technology, Tokyo, Japan, [5]Department of Earth Sciences, University of Minnesota Twin Cities, Minneapolis, Minnesota, USA, [6]Department of Applied Physics and Applied Mathematics, Columbia University, New York, New York, USA, [7]Department of Earth and Environmental Sciences, Lamont-Doherty Earth Observatory - Columbia University, Palisades, New York, USA

Abstract The iron spin crossover in ferropericlase introduces anomalies in its thermodynamics and thermoelastic properties. Here we investigate how these anomalies can affect the lower mantle geotherm using thermodynamics properties from ab initio calculations. The anomalous effect is examined in mantle aggregates consisting of mixtures of bridgmanite, ferropericlase, and $CaSiO_3$ perovskite, with different Mg/Si ratios varying from harzburgitic to perovskitic (Mg/Si ~ 1.5 to 0.8). We find that the anomalies introduced by the spin crossover increase the isentropic gradient and thus the geotherm proportionally to the amount of ferropericlase. The geotherms can be as much as ~200 K hotter than the conventional adiabatic geotherm at deep lower mantle conditions. Aggregate elastic moduli and seismic velocities are also sensitive to the spin crossover and the geotherm, which impacts analyses of lower mantle velocities and composition.

1. Introduction

One of the grand challenges in geophysics is to resolve the thermal structure of the Earth's interior. This is clearly not an isolated problem but a fundamental one to clarify the dynamics, evolution, and chemical stratification of the planet [*McDonough and Sun*, 1995; *Williams and Knittle*, 2005; *Murakami et al.*, 2012]. Besides, a one-dimensional (1-D) temperature profile is an abstract construct—a spherically averaged reference temperature model consistent with spherically averaged velocity and composition profiles. To date, numerous one-dimensional temperature profiles, or geotherms, have been suggested and calculated by various means and using different assumptions. For example, these include seismological observations [*Brown and Shankland*, 1981], mineral physics input [*Anderson*, 1982; *Anzellini et al.*, 2013; *Boehler*, 2000] computations [*da Silva et al.*, 2000; *Karki et al.*, 2001; *Wang et al.*, 2015] or measurements [*Stixrude and Lithgow-Bertelloni*, 2011], geodynamic simulations [*Matyska and Yuen*, 2002; *Bower et al.*, 2009; *Vilella et al.*, 2015], or a combination of them [*Deschamps and Trampert*, 2004; *Hernlund et al.*, 2005]. Differences between them arise not only from the technique or input data but also from the constraints to which they are subjected to, i.e., the melting temperature of iron, phase transitions, seismic discontinuities, convection processes, and lower mantle composition. In addition, lateral velocity heterogeneities point to lateral temperature and/or composition variations, a very difficult problem that still awaits, e.g., advances in geodynamic simulations. Thus, construction of one-dimensional temperature profiles must be seen as an insufficient but a necessary exercise to advance this topic.

An essential aspect in constructing a geotherm is to define a suitable potential temperature, i.e., the boundary condition for integration of the adiabatic gradient. Most geotherms are anchored to depths associated with seismic discontinuities (e.g., the ~660 km discontinuity), where phase transitions occur [*Poirier*, 2000]. For the top of the lower mantle, we assumed a temperature of 1873 K at 23 GPa as in *Brown and Shankland* [1981] (B&S) [see also *Akaogi and Akimoto*, 1979]. The latter is an adiabatic temperature profile constructed from the Debye entropy formulation [*Brillouin*, 1953] and the acoustic velocities from the preliminary reference Earth model (PREM) [*Dziewonski and Anderson*, 1981]. This geotherm is considered by many to be the standard adiabatic geotherm for the lower mantle. It is important to point out that the conditions at

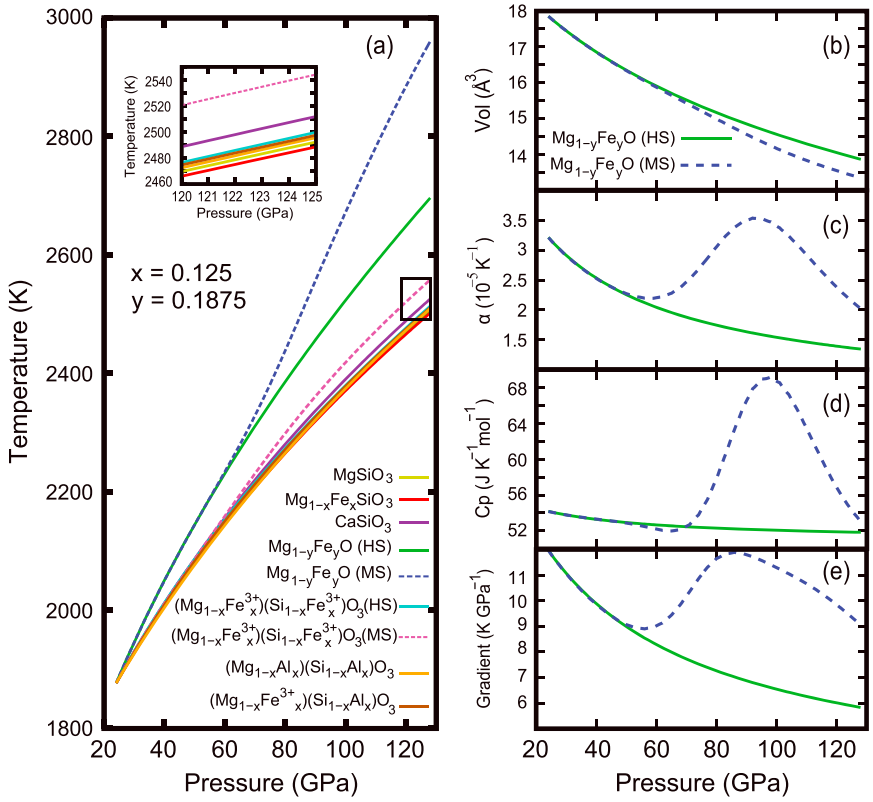

Figure 1. (a) Isentropes for bdg (HS and MS), CaPv, and fp in HS and MS states. Inset corresponds to highlighted region. (b) Volume, (c) thermal expansion coefficient (α), (d) isobaric specific heat (C_P), and (e) adiabatic gradient for fp in HS and MS states.

which ringwoodite dissociates into bridgmanite (bdg) and ferropericlase (fp) are still somewhat controversial [*Irifune et al.*, 1998; *Chudinovskikh and Boehler*, 2001; *Katsura et al.*, 2004; *Ye et al.*, 2014]. Thus, the appropriate potential temperature for the lower mantle geotherm is debatable. Several other geotherms [e.g., *Anderson*, 1982; *Boehler*, 1982; *Anzellini et al.*, 2013] were obtained by extrapolating the temperature from the inner and outer core geotherm using the phase diagram of iron. Additionally, geotherms constructed from ab initio calculations include different approaches; for instance, *da Silva et al.* [2000] and *Karki et al.* [2001] calculated the temperatures needed to fit the bulk modulus of pyrolite to PREM. Others such as *Tsuchiya et al.* [2016] constructed the geotherm from the set of temperatures of different isobars at which the vibrational entropy of bridgmanite was constant.

In this work, we integrated the isentropic gradient formula using thermodynamics properties of minerals obtained by ab initio calculations, starting from the standard boundary condition at 660 km depth, i.e., the experimentally determined postspinel transition conditions [*Akaogi and Akimoto*, 1979], also used by Brown and Shankland [*Brown and Shankland*, 1981]. The relevant lower mantle phases are bdg (Al-Fe-bearing $MgSiO_3$ pervoskite), $CaSiO_3$ perovskite (CaPv), and fp (Mg,Fe)O [*Irifune*, 1994; *Irifune et al.*, 2010; *Murakami et al.*, 2012]. These minerals form a variety of aggregates commonly characterized by their Mg/Si molar ratio. However, the relative abundances of these aggregates in the lower mantle is still debatable [*Irifune*, 1994; *Irifune et al.*, 2010; *Murakami et al.*, 2012; *Wu and Wentzcovitch*, 2014; *Wang et al.*, 2015; *Wu*, 2016]. Here we derived isentropes for likely mantle aggregates such as harzburgite (Mg/Si ~ 1.56) [*Baker and Beckett*, 1999], chondrite (Mg/Si ~ 1.07) [*Hart and Zindler*, 1986], pyrolite (Mg/Si ~ 1.24) [*McDonough and Sun*, 1995], peridotite (Mg/Si ~ 1.30) [*Hirose and Kushiro*, 1993], and perovskite only (Mg/Si ~ 0.82) [*Williams and Knittle*, 2005] to asses the effect of Mg/Si ratio on the isentrope. The presence of FeO in these aggregates needs special consideration. It is well known that ferrous iron (Fe^{+2}) in fp exhibits a spin crossover at lower mantle conditions [*Badro et al.*, 2003; *Speziale et al.*, 2005; *Tsuchiya et al.*, 2006], which introduces anomalies in its thermodynamics [*Wentzcovitch et al.*, 2009; *Wu et al.*, 2009] and thermoelastic properties [*Crowhurst et al.*, 2008; *Marquardt et al.*, 2009; *Antonangeli et al.*, 2011; *Murakami et al.*, 2012; *Wu et al.*, 2013; *Wu and Wentzcovitch*, 2014]. Here we investigated in detail how

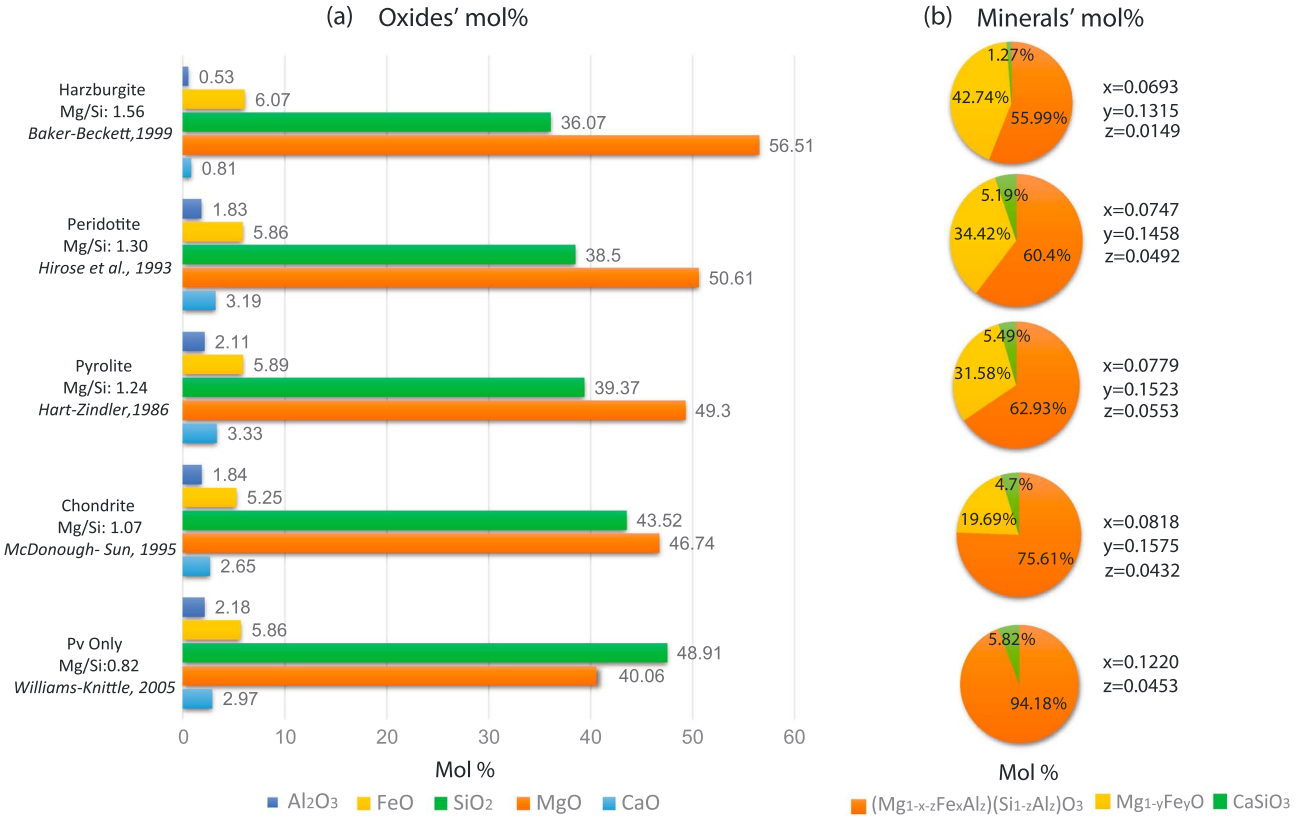

Figure 2. Aggregates characterized by their Mg/Si ratio. (a) Mol % of oxides and (b) minerals in each aggregate. All aggregates have a constant partitioning coefficient K_D of 0.5. The values x, y, and z refer to the concentration of iron in bdg and fp and the concentration of aluminum in bdg.

these anomalies affect the isentropes of these aggregates in the lower mantle. While some geodynamic simulations have shown the potential effect of spin crossover on the lower mantle adiabat [*Bower et al.*, 2009; *Vilella et al.*, 2015], clarification of this effect in the isentropes of several aggregates is a first-order question in advancing the problem of mantle temperatures. Finally, we examined the effect such spin crossover induced thermal anomalies have on aggregate velocities.

2. Method and Calculation Details

The thermoelastic properties of bdg $Mg_{1-x}Fe^{2+}_xSiO_3$, $(Mg_{1-x}Al_x)(Si_{1-x}Al_x)O_3$, $(Mg_{1-x}Fe^{3+}_x)(Si_{1-x}Al_x)O_3$, and $(Mg_{1-x}Fe^{3+}_x)(Si_{1-x}Fe^{3+}_x)O_3$ (x=0 and 0.125) and fp $Mg_{1-y}Fe_yO$ (y = 0 and 0.1875) were obtained from *Shukla et al.* [2015a, 2016] and *Wu et al.* [2013] respectively. Results for other x and y concentrations shown in this work were linearly interpolated and only high spin (HS) Fe^{2+}−bdg was used since no spin crossover in Fe^{2+} occurs in bdg at lower mantle conditions [*Bengtson et al.*, 2009; *Hsu et al.*, 2010; *Hsu and Wentzcovitch*, 2014; *Hsu et al.*, 2011, 2012; *Shukla et al.*, 2015a, 2015b; *Lin et al.*, 2016; *Fukui et al.*, 2016]. For CaPv, thermoelastic properties from *Kawai and Tsuchiya* [2014, 2015] were reproduced within the Mie-Debye-Grüneisen [*Stixrude and Lithgow-Bertelloni*, 2005] formalism (see the supporting information). We considered mixtures of SiO_2 - MgO - CaO - FeO - Al_2O_3 for relevant mantle aggregates; namely, harzburgite [*Baker and Beckett*, 1999], chondrite [*Hart and Zindler*, 1986], pyrolite [*McDonough and Sun*, 1995], peridotite [*Hirose and Kushiro*, 1993], and perovskitic only [*Williams and Knittle*, 2005].

Although the Fe-Mg partitioning coefficient $K_D = \frac{x/(1-x-z)}{y/(1-y)}$ between bdg and fp is expected to vary throughout the lower mante because of spin crossover [*Irifune et al.*, 2010; *Piet et al.*, 2016], we have examined compositions with a uniform K_D with values of 0.5 and 0.25. For the aggregates shown in this manuscript, a K_D of 0.5 was used as it is more consistent with those reported by *Irifune et al.* [2010] and *Piet et al.* [2016]. Aggregate adiabats with K_D of 0.25 are shown in the supporting information. Also, we show in Tables S1 and S2 the weight, molar, and volume percentages of oxides and minerals in the aggregates considered and in Tables S3 and S4 their corresponding adiabats.

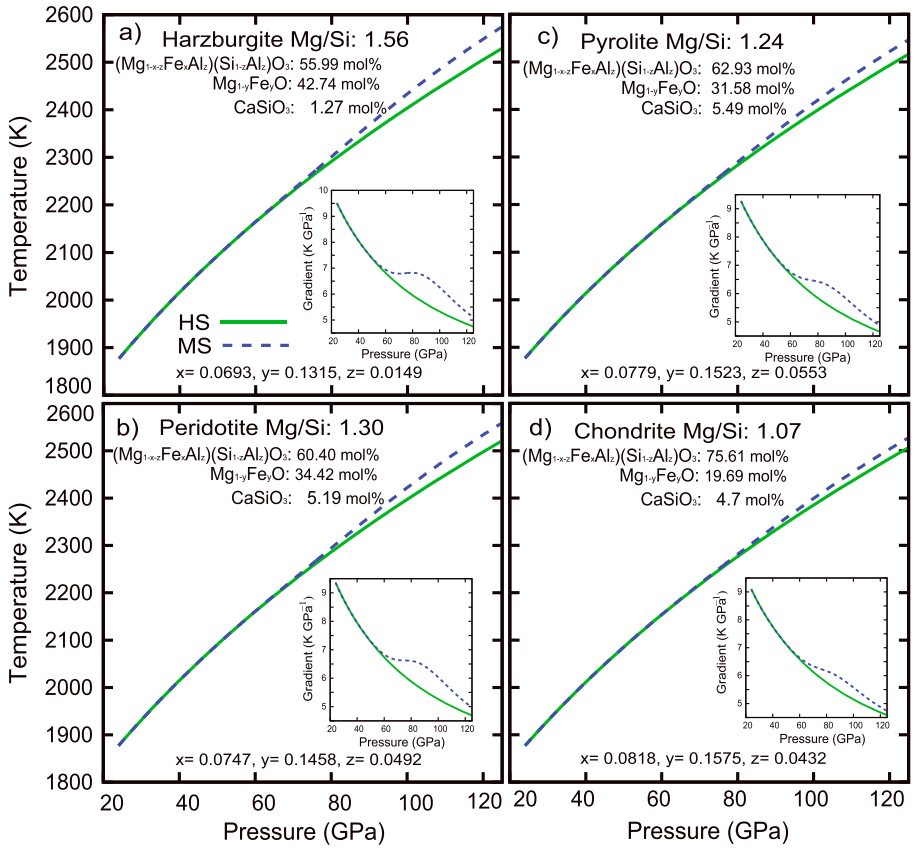

Figure 3. Adiabats for (a) harzburgite, (b) peridotite, (c) pyrolite, and (d) chondrite with fp in HS and MS states. The values *x*, *y*, and *z* refer to the concentration of iron in bdg and fp and the concentration of aluminum in bdg. Solid/dashed lines correspond to adiabats with fp in HS/MS states. Inset figures show the adiabatic gradient for each aggregate.

The isentropes of different minerals and aggregates were found from their isentropic gradients computed as follows:

$$\left(\frac{\partial T}{\partial P}\right)_S = \frac{\alpha_{\text{agg}} V_{\text{agg}} T}{C_{p_{\text{agg}}}}, \tag{1}$$

where the aggregate quantities $V_{\text{agg}} = \sum_i \phi_i V_i$, $\alpha_{\text{agg}} = \sum_i \alpha_i \phi_i V_i / V_{\text{agg}}$, and $C_{p_{\text{agg}}} = \sum_i \phi_i C_{p_i}$ are the aggregate volume, thermal expansion coefficient, and isobaric specific heat, respectively. Here ϕ_i, V_i, α_i, and Cp_i represent, respectively, the molar fraction, molar volume, thermal expansion coefficient, and isobaric specific heat of the *i*th mineral in the mixture. All the isentropes, here loosely referred as geotherms, were compared with the adiabatic [*Brown and Shankland*, 1981] and superadiabatic [*Anderson*, 1982] geotherms. Once these geotherms were obtained, we computed aggregate velocities along aggregate specific geotherms using the Voigt-Reuss-Hill average of elastic moduli and compared with PREM values [*Dziewonski and Anderson*, 1981].

Uncertainties resulting from our ab initio calculations due to k-point sampling, energy cutoff, and exchange correlations are systemic in nature. Therefore, if such uncertainties induced further uncertainties in the calculated temperature profiles, these were consistently introduced in each of the minerals of a given aggregate. Thus, the overall conclusion of this study is unlikely to change irrespective of such uncertainties.

3. Results and Discussion

3.1. Lower Mantle Mineral Isentropes

To unravel the possible consequences of the iron spin crossover in fp (and bdg) on the lower mantle geotherm, first we calculated using equation (1), the isentropes of $(Mg_{0.875}Fe_{0.125})SiO_3$, $(Mg_{0.875}Al_{0.125})(Si_{0.875}Al_{0.125})O_3$, $(Mg_{0.875}Fe^{3+}_{0.125})(Si_{0.875}Al_{0.125})O_3$, $(Mg_{0.875}Fe^{3+}_{0.125})(Si_{0.875}Fe^{3+}_{0.125})O_3$, $CaSiO_3$, and $(Mg_{0.8125}Fe_{0.1875})O$, with iron in high spin (HS) state and in a mixed spin (MS) state of HS and low spin (LS) states (see Figure 1).

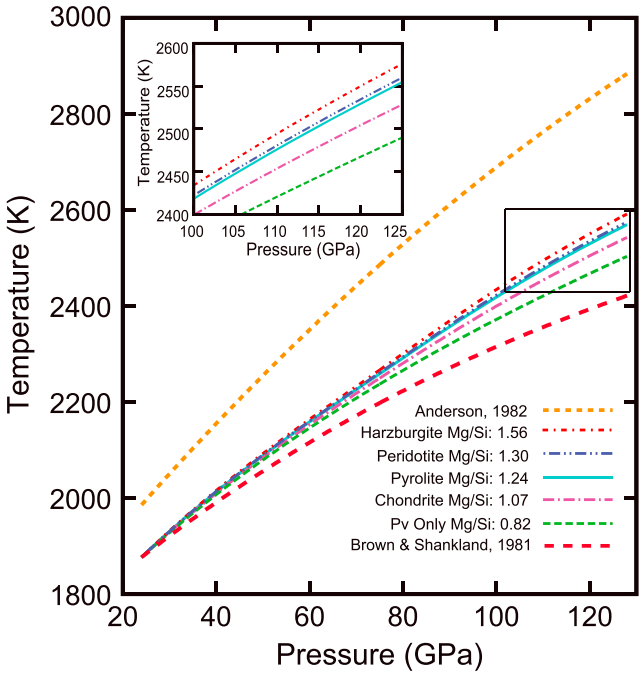

Figure 4. Calculated adiabats for aggregates considered, compared with geotherms by *Brown and Shankland* [1981] and *Anderson* [1982]. Inset corresponds to highlighted region.

Here temperature differences among all the different bdgs in HS are only about ~2 K at 125 GPa, while differences with bdg in MS state (~50 K) and $CaSiO_3$ (~20 K) were more significant (see Figure 1a). For fp however, the isentropes in MS and HS states differ by ~260 K at deep lower mantle pressures (Figure 1a). Hence, spin crossover in fp induces the most dramatic effect on the lower mantle temperature profile. The anomalies caused by the spin crossover on V, α, and C_p (see Figures 1b–1d) on the adiabatic gradient of fp (Figure 1e) are responsible for such temperature increase. Note that for α and C_p, the spin crossover anomalies correspond to broad peaks at similar pressure ranges but do not cancel during the adiabatic gradient integration owing to significant differences in their magnitudes (Figures 1c and 1d).

3.2. Effect of Mg/Si Ratio and fp Spin Crossover on the Geotherm

We now investigate the isentropes of aggregates likely to be present in the lower mantle. Their compositions are shown in Figure 2. The horizontal charts in Figure 2a represent the oxides mol % of SiO_2 - MgO - CaO - FeO - Al_2O_3 in the aggregate, while the pie charts in Figure 2b show the mol % of each mineral (bdg, fp, and CaPv) in the aggregate. Each composition is characterized by its Mg/Si molar ratio, and it is clear that as Mg/Si decreases, so does the amount of fp. Further details about these compositions can be found in the supporting information.

In what follows, we did not include Fe_2O_3 in any of the aggregates since the oxygen fugacity of the deep mantle, and thus the amount of ferric iron (Fe^{3+}), is still an open question beyond the scope of this manuscript. However, we investigated the possible effect of spin crossover in bdg on a pyrolitic composition (see Figure S10). Here we assumed that all iron in bdg is ferric and equally distributed into its A and B sites. Spin crossover in bdg increases the temperature by ~13 K in this case. Furthermore, in the presence of Al_2O_3, ferric iron is expected to enter into the A site of bdg and spin crossover gets suppressed in this case [*Hsu et al.*, 2011, 2012; *Shukla et al.*, 2016; *Shukla and Wentzcovitch*, 2016]. Moreover, as it was shown in Figure 1a, the isentropes of $(Mg_{1-x}Fe^{3+}_x)(Si_{1-x}Al_x)O_3$ and $(Mg_{1-x}Fe^{2+}_x)SiO_3$ only differ by ~6 K at 125 GPa, and therefore, the aggregate adiabats between these cases will not vary significantly.

We used the CaPv thermoelastic properties from *Kawai and Tsuchiya* [2014, 2015], which are not in the best agreement with recent experimental results conducted by *Sun et al.* [2016] (Figure S8). This choice of CaPv was made for consistency since *Kawai and Tsuchiya* [2014, 2015] reported a shear modulus, which not only is significantly smaller than that reported by *Stixrude and Lithgow-Bertelloni* [2011] (Figure S7) but also helped to reduce discrepancies with PREM values for all aggregates containing CaPv. Besides, the CaPV parameters reported by *Sun et al.* [2016] did not introduce any major difference (less than ~2 K at 125 GPa) when implemented to calculate the aggregate adiabat (Figure S5b).

We first examined the temperature increments caused by the spin crossover in all aggregates in which fp does (MS) and does not (HS) undergo spin crossover (Figure 3). Adiabatic geotherms and gradients (insets) are shown in Figures 3a–3d. The temperature differences between HS and MS at high pressures (P ~125 GPa) for harzburgite (~50 K) were greater than those for peridotite (~40 K), pyrolite (~30 K), and chondrite (~20 K)

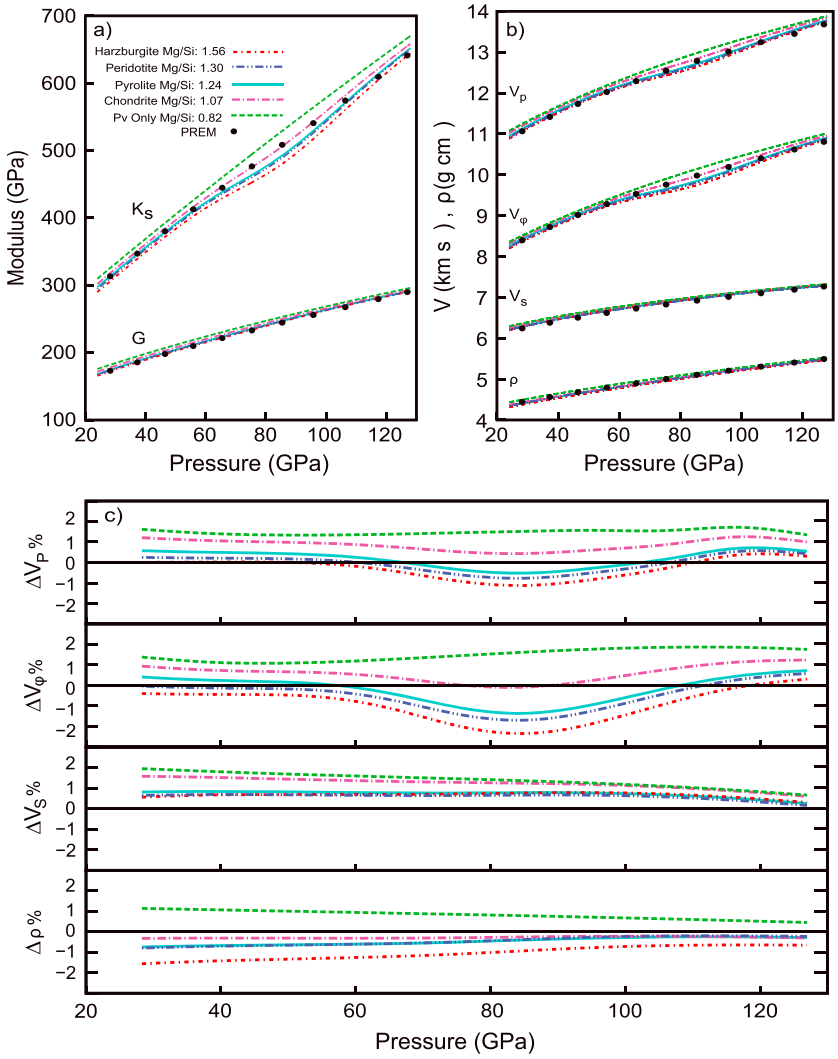

Figure 5. (a) Elastic moduli (K_S, G), (b) acoustic velocities (V_P, V_ϕ, V_S), and densities (ρ) for all aggregates considered. Black circles indicate PREM values [*Dziewonski and Anderson*, 1981]. (c) Relative deviations from PREM shown as percentages.

owing to harzburgite's higher Mg/Si. We also notice that MS gradients (insets) for all aggregates deviate from HS at pressures of ~60 GPa, as a consequence of the spin crossover, and the gradient decreases in proportion to the Mg/Si ratio.

The isentropes of all aggregates were compared with reference geotherms by *Brown and Shankland* [1981] and *Anderson* [1982] in Figure 4. All calculated adiabats were anchored to 1873 K at 23 GPa as in *Akaogi and Akimoto* [1979] and *Brown and Shankland* [1981]. At deep lower mantle conditions, harzburgite achieves the highest temperature, which is about ~200 K higher than that of B&S. Temperatures then decrease with Mg/Si ratio, i.e., the aggregate's fp fraction. Such temperature variations are also expected when K_D is reduced, i.e., fp containing a higher iron content. For this scenario, the crossover anomaly in the adiabat variables (α, C_p, and V) will be more pronounced and consequently leading to hotter temperatures (see Figure S9).

The relative temperature differences $\Delta T/T$ between fp in MS and HS states from geodynamic simulations [*Bower et al.*, 2009; *Vilella et al.*, 2015] are in overall agreement with our predictions despite the differences in the details of the aggregate's K_D and calculations. For instance, simulations by *Bower et al.* [2009] using $Mg_{83}Fe_{17}O$ indicated a maximum relative temperature difference $\Delta T/T$ of ~10% at 113 GPa (~2500 km depth). As shown in Figure 1a, the temperature difference at 113 GPa between fp in MS and HS states is about ~200 K, which corresponds to a $\Delta T/T \sim 8\%$. Given the different nature and details of these calculations, the agreement is outstanding. Furthermore, at the same pressure of 113 GPa, geodynamic simulations

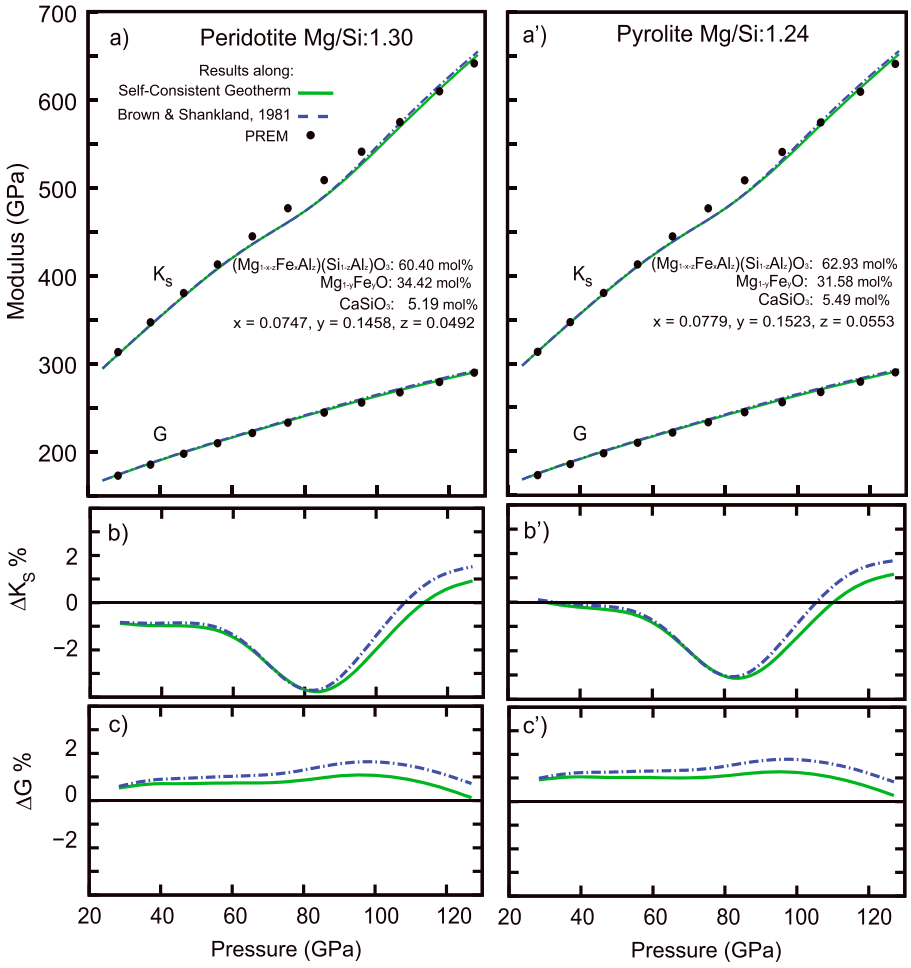

Figure 6. Elastic moduli (K_S, G) for (a) peridotite and (a') pyrolite along self-consistent (solid green line) and *Brown and Shankland* [1981] (dashed blue line) geotherms. Black circles correspond to PREM values [*Dziewonski and Anderson*, 1981]. (b/b' and c/c') are the elastic moduli relative deviations (ΔK_S% and ΔG%) with respect to PREM values, shown as percentages for peridotite/pyrolite.

by *Vilella et al.* [2015] inferred a MS-HS temperature difference of ~20 K ($\Delta T/T \sim$ 0.6%) and 50 K ($\Delta T/T \sim$ 1.6%) for Al-bearing and Al-free pyrolite aggregates, respectively. Our results showed a temperature increment of ~27 K, which corresponds to $\Delta T/T \sim$ 1.1%, for both Al-bearing (Figure 3c) and Al-free pyrolite. However, the MS-HS comparisons by *Vilella et al.* [2015] were done for the same aggregate with different K_D, i.e., their Al-free pyrolite in HS had a K_D of 0.4 and in MS of 0.02, while for Al-bearing pyrolite, K_D was 0.5 and 0.4 for HS and MS, respectively. Despite the differences in details, there is also a good overall agreement in this case.

4. Geophysical Significance

The elastic moduli (K_S, G), acoustic velocities (V_P, V_ϕ, and V_S), and densities (ρ) of all the aggregates along their own isentropes are shown in Figure 5. In aggregates containing fp, K_S softening due fp spin crossover [*Wu et al.*, 2013; *Wu and Wentzcovitch*, 2014] is observed and varies proportionally to the Mg/Si ratio (Figure 5a). Moreover, G does not exhibit any anomalous behavior and its value for different compositions converges to similar values at deep lower mantle pressures. For aggregates with higher Mg/Si ratio, calculated G revealed a better agreement with PREM values, while the K_S values for chondrite and pyrolite were closer to PREM values (Figure 5a). The signature of K_S anomalies was also obvious in the compressional ($V_p = \sqrt{(K_S + \frac{4}{3}G)/\rho}$) and bulk ($V_\phi = \sqrt{K_S/\rho}$) velocities, while shear velocities $V_S = \sqrt{G/\rho}$ were unaffected (see Figure 5b).

The relative velocity deviations (ΔV_P%, ΔV_ϕ%, and ΔV_S%) from PREM values are shown in Figure 5c. ΔV_P% and ΔV_ϕ% decreased with increasing Mg/Si ratio and reached negative values mainly due fp spin crossover.

However, ΔV_S% for all the aggregates was positive and the deviations from PREM values for pyrolite, perditotite, and harzburgite were the lowest (less than 1%). The relative density deviations ($\Delta\rho$) reduced with increasing pressure (Figure 5c). For compositions with fp, the volume collapse caused by fp spin crossover [*Wentzcovitch et al.*, 2009] seemed to reduce such deviations further.

Moreover, as discussed in section 3.2, the iron spin crossover in fp raises the aggregate's geotherm in proportion to its fp content (or to the iron content in fp). This temperature boost can affect analyses of the lower mantle composition. Figures 6a and 6a′ show peridotite and pyrolite's elastic moduli along their own geotherms and the B&S geotherm. Although not substantial, relative deviations from PREM varied depending on the geotherm used. For the bulk modulus ΔK_S% in Figures 6b and 6b′, the relative deviations from PREM were the same along both geotherms until pressures lower than 80 GPa, while for the shear modulus relative deviations ΔG%, results along the self-consistent geotherm (Figures 6c and 6c′) exhibited lower deviations from PREM throughout the whole lower mantle. Such details suggest that the aggregate thermoelastic properties along the self-consistent geotherm should sharpen uncertainties in analyses of lower mantle composition.

5. Conclusions

We presented a set of adiabatic geotherms for individual minerals and likely lower mantle aggregates under realistic pressure and temperature conditions. We showed that the spin crossover in ferropericlase introduces an anomaly in its isentrope similar to "superadiabaticity." This effect increased the adiabatic temperature gradient in different aggregates in proportion to their ferropericlase content or Mg/Si ratio. Velocities of aggregates with compositions varying from perovskitic to harzburgitic along their self-consistent geotherms exhibited deviations from PREM velocities within $\pm$ ~2%. However, pyrolitic and peridotitic compositions displayed the best fit with respect to PREM values. The elastic moduli, velocities, and densities of these aggregates along their own self-consistent geotherms tend to display smaller deviations from PREM (up to ~1% less) than those along standard geotherms such as *Brown and Shankland* [1981]. We stress here that we cannot afford to ignore the impact from the spin crossover anomalies, because neglecting them would lead to erroneous interpretations of the lower mantle geotherm and composition.

Acknowledgments
The authors acknowledge Caroline Qian for her early contributions to the isentrope code. This work was supported primarily by grants NSF/EAR1319368 and 1348066 and NSF/CAREER1151738. Zhongqing Wu was supported by State Key Development Program of Basic Research of China (2014CB845905) and NSF of China (41274087). C. Houser was supported by the Earth-Life Science Institute at Tokyo Institute of Technology. Results produced in this study are available in the supporting information.

References

Akaogi, M., and S. Akimoto (1979), High-pressure phase equilibria in a garnet lherzolite, with special reference to Mg^{2+} Fe^{2+} partitioning among constituent minerals, *Phys. Earth Planet. Inter.*, *19*, 31–51.

Anderson, O. L. (1982), The Earth's core and phase diagram of iron, *Philos. Trans. R. Soc. London, Ser. A*, *306*, 21–35.

Antonangeli, D., J. Siebert, C. M. Aracne, D. L. Farber, A. Bosak, M. Hoesch, M. Krisch, F. J. Ryerson, G. Fiquet, and J. Badro (2011), Spin crossover in ferropericlase at high pressure: A seismologically transparent transition?, *Science*, *331*, 64–67.

Anzellini, S., A. Dewaele, M. Mezouar, P. Loubeyre, and G. Morard (2013), Melting of iron at Earth's inner core boundary based on fast X-ray diffraction, *Science*, *340*, 464–466.

Badro, J., G. Fiquet, F. Guyot, J. P. Rueff, V. V. Struzhkin, Vankó G., and G. Monaco (2003), Iron partitioning in Earth's mantle: Toward a deep lower mantle discontinuity, *Science*, *300*, 789–791.

Baker, M. B., and J. R. Beckett (1999), The origin of abyssal peridotites: A reinterpretation of constraints based on primary bulk compositions, *Earth Planet. Sci. Lett.*, *171*, 49–61.

Bengtson, A., J. Li, and D. Morgan (2009), Mössbauer modeling to interpret the spin state of iron in (Mg, Fe)SiO_3 perovskite, *Geophys. Res. Lett.*, *36*, L15301, doi:10.1029/2009GL038340.

Boehler, R. (2000), High-pressure experiments and the phase diagram of lower mantle and core materials, *Rev. Geophys.*, *2*, 221–245, doi:10.1029/1998RG000053.

Bower, D. J., M. Gurnis, J. M. Jackson, and W. Sturhahn (2009), Enhanced convection and fast plumes in the lower mantle induced by the spin transition in ferropericlase, *Geophys. Res. Lett.*, *36*, L10306, doi:10.1029/2009GL037706.

Brillouin, L. (1953), *Wave Propagation in Periodic Structures: Electric Filters and Crystal Lattices*, 2nd ed., Dover Publ.

Brown, J. M., and T. J. Shankland (1981), Thermodynamic parameters in the Earth as determined from seismic profiles, *Geophys. J. R. Astron. Soc.*, *66*, 579–596.

Chudinovskikh, L., and R. Boehler (2001), High-pressure polymorphs of olivine and the 660-km seismic discontinuity, *Nature*, *411*, 574–577.

Crowhurst, J. C., J. M. Brown, A. F. Goncharov, and S. D. Jacobsen (2008), Elasticity of (Mg, Fe) O through the spin transition of iron in the lower mantle, *Science*, *319*, 451–453.

da Silva, C. R. S., R. M. Wentzcovitch, A. Patel, G. D. Price, and S. I. Karato (2000), The composition and geotherm of the lower mantle: Constraints from the elasticity of silicate perovskite, *Phys. Earth Planet. Int.*, *118*, 103–109.

Deschamps, F., and J. Trampert (2004), Towards a lower mantle reference temperature and composition, *Earth Planet. Sci. Lett.*, *222*, 161–175.

Dziewonski, A. M., and D. L. Anderson (1981), Preliminary reference Earth model, *Phys. Earth Planet. Int.*, *25*, 297–356.

Fukui, H., et al. (2016), Effect of cation substitution on bridgmanite elasticity: A key to interpret seismic anomalies in the lower mantle, *Sci. Rep.*, *6*, 33337, doi:10.1038/srep33337.

Hart, S. R., and A. Zindler (1986), In search of a bulk-Earth composition, *Chem. Geol.*, *57*, 247–267, doi:10.1016/0009-2541(86)90053-7.

Hernlund, J. W., C. Thomas, and P. J. Tackley (2005), A doubling of the post-perovskite phase boundary and structure of the Earth's lowermost mantle, *Nature*, *434*, 882–886.

Hirose, K., and I. Kushiro (1993), Partial melting of dry peridotites at high pressures: Determination of compositions of melts segregated from peridotite using aggregates of diamond, *Earth Planet. Sci. Lett.*, *114*, 477–489.
Hsu, H., and R. M. Wentzcovitch (2014), First-principles study of intermediate-spin ferrous iron in the Earth's lower mantle, *Phys. Rev. B*, *90*, 195205, doi:10.1103/PhysRevB.90.195205.
Hsu, H., K. Umemoto, P. Blaha, and R. M. Wentzcovitch (2010), Spin states and hyperfine interactions of iron in (Mg,Fe)SiO_3 perovskite under pressure, *Earth Planet. Sci. Lett.*, *294*, 19–26.
Hsu, H., P. Blaha, M. Cococcioni, and R. M. Wentzcovitch (2011), Spin-state crossover and hyperfine interactions of ferric iron in $MgSiO_3$ perovskite, *Phys. Rev. Lett.*, *106*, 118501.
Hsu, H., G. Y. Yonggang, and R. M. Wentzcovitch (2012), Spin crossover of iron in aluminous $MgSiO_3$ perovskite and post-perovskite, *Earth Planet. Sci. Lett.*, *359*, 34–39.
Irifune, T. (1994), Absence of an aluminous phase in the upper part of the Earth's mantle, *Nature*, *370*(1994), 131–133.
Irifune, T., et al. (1998), The postspinel phase boundary in Mg_2SiO_4 determined by in situ X-ray diffraction, *Science*, *279*(1998), 1698–1700.
Irifune, T., T. Shinmei, C. A. McCammon, N. Miyajima, D. C. Rubie, and D. J. Frost (2010), Iron partitioning and density changes of pyrolite in Earth's lower mantle, *Science*, *327*, 193–195.
Karki, B., R. Wentzcovitch, S. de Gironcoli, and S. Baroni (2001), First principles thermoelasticity of $MgSiO_3$-perovskite: Consequences for the inferred properties of the lower mantle, *Geophys. Res. Lett.*, *28*, 2699–2702, doi:10.1029/2001GL012910.
Katsura, T., et al. (2004), Olivine-wadsleyite transition in the system (Mg, Fe)$_2SiO_4$, *J. Geophys. Res.*, *109*, B02209, doi:10.1029/2003JB002438.
Kawai, K., and T. Tsuchiya (2014), P-V-T equation of state of cubic $CaSiO_3$ perovskite from first-principles computation, *J. Geophys. Res. Solid Earth*, *119*, 2801–2809, doi:10.1002/2013JB010905.
Kawai, K., and T. Tsuchiya (2015), Small shear modulus of cubic $CaSiO_3$ perovskite, *Geophys. Res. Lett.*, *42*, 2718–2726, doi:10.1002/2015GL063446.
Lin, J., Z. Mao, J. Yang, J. Liu, Y. Xiao, P. Chow, and T. Okuchi (2016), High-spin and Fe^{2+} and Fe^{3+} in single-crystal aluminous bridgmanite in the lower mantle, *Geophys. Res. Lett.*, *43*, 6952–6959, doi:10.1002/2016GL069836.
Marquardt, H., S. Speziale, H. J. Reichmann, D. J. Frost, F. R. Schilling, and E. J. Garnero (2009), Elastic shear anisotropy of ferropericlase in Earth's lower mantle, *Science*, *324*, 224–226.
Matyska, C., and D. A. Yuen (2002), Bullen's parameter η: A link between seismology and geodynamical modelling, *Earth Planet. Sci. Lett.*, *198*, 471–483.
McDonough, W. F., and S. S. Sun (1995), The composition of the Earth, *Chem. Geol.*, *120*, 223–253, doi:10.1016/0009-2541(94)00140-4.
Murakami, M., Y. Ohishi, N. Hirao, and K. Hirose (2012), A perovskitic lower mantle inferred from high-pressure, high-temperature sound velocity data, *Nature*, *485*, 90–94, doi:10.1038/nature11004.
Piet H., J. Badro, F. Nabiei, T. Dennenwaldt, S. H. Shim, M. Cantoni, C. Hébert, and P. Gillet (2016), Spin and valence dependence of iron partitioning in Earth's deep mantle, *Proc. Natl. Acad. Sci. U.S.A.*, *113*, 11,127–11,130.
Poirier, J. P. (2000), *Introduction to the Physics of Earth's Interior*, 2nd ed., Cambridge Univ. Press, New York.
Shukla, G., and R. M. Wentzcovitch (2016), Spin crossover in (Mg, Fe^{3+})(Si, Fe^{3+}) O_3 bridgmanite: Effects of disorder, iron concentration, and temperature, *Phys. Earth Planet. Inter.*, *260*, 53–61, doi:10.1016/j.pepi.2016.09.003.
Shukla, G., Z. Wu, H. Hsu, A. Floris, M. Cococcioni, and R. M. Wentzcovitch (2015a), Thermoelasticity of Fe^{2+}-bearing bridgmanite, *Geophys. Res. Lett.*, *42*, 1741–1749, doi:10.1002/2014GL062888.
Shukla, G., M. Topsakal, and R. M. Wentzcovitch (2015b), Spin crossovers in iron-bearing $MgSiO_3$ and $MgGeO_3$: Their influence on the post-perovskite transition, *Phys. Earth Planet. Inter.*, *249*, 11–17, doi:10.1016/j.pepi.2015.10.002.
Shukla, G., M. Cococcioni, and R. M. Wentzcovitch (2016), Thermoelasticity of Fe^{3+}- and Al-bearing bridgmanite, *Geophys.Res. Lett.*, *43*, 5661–5670, doi:10.1002/2016GL069332.
Speziale, S., A. Milner, V. E. Lee, S. M. Clark, M. P. Pasternak, and R. Jeanloz (2005), Iron spin transition in Earth's mantle, *Proc. Natl. Acad. Sci. U.S.A.*, *102*, 17918–17922.
Stixrude, L., and C. Lithgow-Bertelloni (2005), Thermodynamics of mantle minerals—I. Physical properties, *Geophys. J. Int.*, *162*, 610–632.
Stixrude, L., and C. Lithgow-Bertelloni (2011), Thermodynamics of mantle minerals—II. Phase equilibria, *Geophys. J. Int.*, *184*, 1180–1213.
Sun, N., Z. Mao, S. Yan, X. Wu, V. B. Prakapenka, and J. F. Lin (2016), Confirming a pyrolitic lower mantle using self-consistent pressure scales and new constraints on $CaSiO_3$ perovskite, *J. Geophys. Res. Solid Earth*, *121*, 4876–4894, doi:10.1002/2016JB013062.
Tsuchiya, T., R. M. Wentzcovitch, C. R. da Silva, and S. de Gironcoli (2006), Spin transition in magnesiowüstite in Earth's lower mantle, *Phys. Rev. Lett.*, *96*, 198501.
Tsuchiya, T., K. Kawai, X. Wang, H. Ichikawa, and H. Dekura (2016), Temperature of the lower mantle and core based on ab initio mineral physics data, in *Deep Earth: Physics and Chemistry of the Lower Mantle and Core*, pp. 13–30, John Wiley, Hoboken, N. J., doi:10.1002/9781118992487.
Vilella, K., S. H. Shim, C. G. Farnetani, and J. Badro (2015), Spin state transition and partitioning of iron: Effects on mantle dynamics, *Earth Planet. Sci. Lett.*, *417*, 57–66, doi:10.1016/j.epsl.2015.02.009.
Wang, X., T. Tsuchiya, and A. Hase (2015), Computational support for a pyrolitic lower mantle containing ferric iron, *Nat. Geosci.*, *8*, 556–559, doi:10.1038/ngeo2458.
Wentzcovitch, R. M., J. F. Justo, Z. Wu, C. R. S da Silva, A. Yuen, and D. Kohlstedtd (2009), Anomalous compressibility of ferropericlase throughout the iron spin cross-over, *Proc. Natl. Acad. Sci. U.S.A.*, *106*, 8447–8452.
Williams, Q., and E. Knittle (2005), The uncertain major element bulk composition of Earth's mantle, in *Earth's Deep Mantle: Structure, Composition, and Evolution, Geophys. Monogr. Ser.*, vol.160, AGU, Washington, D. C., doi:10.1029/160GM12.
Wu, Z. (2016), Velocity structure and composition of the lower mantle with spin crossover in ferropericlase, *J. Geophys. Res. Solid Earth*, *121*, 2304–2314, doi:10.1002/2015JB012667.
Wu, Z., and R. M. Wentzcovitch (2014), Spin crossover in ferropericlase and velocity heterogeneities in the lower mantle, *Proc. Natl. Acad. Sci. U.S.A.*, *111*, 10,468–10,472.
Wu, Z., J. F. Justo, C. R. S da Silva, S de Gironcoli, and R. M. Wentzcovitch (2009), Anomalous thermodynamic properties in ferropericlase throughout its spin crossover transition, *Phys. Rev. B.*, *80*, 14409.
Wu, Z., J. F. Justo, and R. M. Wentzcovitch (2013), Elastic anomalies in a spin-crossover system: Ferropericlase at lower mantle conditions, *Phys. Rev. Lett.*, *110*, 228501.
Ye, Y., C. Gu, S. H. Shim, Y. Meng, and V. Prakapenka (2014), The postspinel boundary in pyrolitic compositions determined in the laser-heated diamond anvil cell, *Geophys. Res. Lett.*, *41*, 3833–3841, doi:10.1002/2014GL060060.